

# Effective potentials for polymers and colloids: Beyond the van der Waals picture of fluids?

BY A.A. LOUIS

*Department of Chemistry, Lensfield Rd, Cambridge CB2 1EW, UK*

This contribution briefly reviews some recent work demonstrating the partial breakdown of the colloidal fluid  $\leftrightarrow$  atomic fluid analogy. The success of liquid state theory for atomic fluids stems in part from the van der Waals picture, where steric interactions dominate the structure, and attractive interactions can be added as a perturbation. For complex fluids described by effective potentials, this picture may break down. In the first example discussed, depletion potentials in non-additive hard-sphere mixtures are shown to be surprisingly complex, leading to fluid structure and fluid-solid transitions dominated by properties of the attractive potentials instead of by the hard-cores. Many colloidal suspensions, and possibly globular proteins, fall into this *energetic fluid* category. In the second example, the coarse-graining of polymers leads to soft-core effective potentials and associated *mean field fluid* behaviour distinguished by a breakdown of the virial expansion, an equation of state that is nevertheless nearly linear in density, and correlation functions well described by the random phase approximation.

**Keywords:** effective potentials, depletion, colloidal suspensions, colloid-polymer mixtures, simple fluids, globular proteins

## 1. Introduction

Integrating out a subset of the degrees of freedom (i.e. coarse-graining) is the first step in many analyses of soft matter systems. For colloidal and polymeric suspensions, this procedure often leads to *effective potentials*, and much progress has emerged from exploiting the analogy between these potentials and the potentials of atomic and molecular fluids. In fact, the basic philosophy behind effective potentials is that the initial effort in deriving them is recouped when they are input into the well-oiled machinery of liquid state theory. However, coarse-graining on the wide range of length scales available in soft-matter systems leads to a much richer class of potentials than those found for their atomic and molecular counterparts (Likos 2001). Since liquid state theory was originally derived and optimized for the latter, this immediately implies the possible breakdown of the soft-matter  $\leftrightarrow$  atomic fluids analogy.

This paper will focus on a careful derivation of the effective pair potentials for colloid-colloid, polymer-colloid and pure polymer suspensions, with a special emphasis on examples where intuition gleaned from the atomic fluid analogy begins to fail.

In the first example discussed, depletion potentials are derived for highly asymmetric non-additive binary hard sphere (HS) mixtures. It is argued that these potentials can describe a much wider class of asymmetric binary mixtures and lead, in the low density regime of the larger species, to *energetic fluids*, where the structure and crystallization behaviour is dominated by the effective potentials rather than the hard cores. For this reason, a careful derivation of the effective potentials is particularly important.

The second example concerns modelling polymers as “soft colloids”. These are represented by potentials *without hard cores*, leading to the concept of *mean-field fluids*, with behaviour quite different from the HS paradigm that underpins the theory of simple liquids.

## 2. The van der Waals picture of fluids

But first, let us take a careful look at the theory of simple liquids (Hansen & McDonald 1986): Why has it been so successful? Perhaps the primary factor is the surprisingly widespread applicability of the HS fluid as a model of steric effects in atomic and molecular fluids. Attractive forces can then be added as a perturbation to a HS reference system. This approach is sometimes called the *van der Waals picture* of fluids<sup>†</sup>, and a clear summary statement appeared in an influential review (Chandler *et al.* 1983):

According to the van der Waals picture, the average relative arrangements and motions of molecules in a liquid (that is the intermolecular structure and correlations) are determined primarily by the local packing and steric effects produced by the short-ranged repulsive intermolecular forces. Attractive forces, dipole-dipole interactions, and other slowly varying interactions, all play a minor role in the structure, and in the simplest approximation their effect can be treated in terms of a mean-field – a spatially uniform background potential – which exerts no intermolecular force and hence has no effect on the structure or dynamics, but merely provides the cohesive energy that makes the system stable at a particular density or pressure.

Historically, the 1957 discovery of a first order freezing transition in a pure hard-sphere system (Alder & Wainwright 1957; Wood & Jacobson 1957) really got the metaphorical ball rolling, but other early highlights include:

- **Freezing:** Longuet-Higgins & Widom (1964) and Widom (1967) showed that attractive interactions only mildly perturb the HS freezing transition near the triple point.
- **Structure:** Ashcroft and Lekner (1966), and Verlet (1967), modelled the structure factor  $S(k)$  of liquid metals and many other fluids by the HS  $S(k)$  at an appropriate effective HS diameter. Hansen and Verlet (1969) then connected structure to freezing by deriving a criterion — the first maximum peak of  $S(k)$  has a value of about 2.8 near the freezing transition — that holds not only for HS fluids, but also for a much wider set of atomic fluids.

<sup>†</sup> The term van der Waals plus the term fluid appear in various combinations in the literature. Its use here follows the definition found in the Chandler, Weeks & Andersen (1983) review.

These ideas were put on a firmer footing by the Barker-Henderson perturbation theory (Barker & Henderson 1967), and the more systematic Weeks–Chandler–Andersen theory of liquids (Chandler & Weeks 1970; Weeks *et al.* 1971). Both theories provide ways of performing quantitative calculations for fluids based on a HS reference system plus a perturbative term arising from the attractions. That these concepts can also be extended to molecular fluids with non-spherical hard-core reference systems is illustrated by a second, more whimsical, citation from the Chandler, Weeks, & Andersen (1983) review:

Similarly the arrangements of molecules in liquid benzene are similar to the average arrangements of neighboring Cheerios in a bowl of breakfast cereal, and a solution of argon in benzene should be similar to the structure achieved when blueberries are mixed with Cheerios.

The upshot of all this is that near the triple point, the region for which liquid state theory was optimised, the structure and thermodynamics of atomic and molecular fluids is dominated by the underlying hard-core system; the effect of attractive potentials is *quantitative*, but not *qualitative* (at least for freezing and structure). This is no longer true for complex fluids. Instead, as we shall see in the following sections of this paper, effective potentials may induce *qualitative changes* in the structure and thermodynamics of soft matter systems. The van der Waals picture breaks down.

### 3. Example A: Depletion potentials lead to “Energetic” Fluids

#### (a) Depletion potentials for non-additive binary hard-sphere mixtures

Depletion interactions, the effective entropic potentials induced between the remaining particles when one (repulsive and typically smaller) component is integrated out, were first described by Asakura & Oosawa (1954, 1958). They remained largely unexplored until around 25 years ago when the experiments of Vincent and co-workers (Li-In-On *et al.* 1975) and the theoretical work of Vrij (1976) rekindled interest. Since then, there has been a steadily increasing body of work exploiting the “tunability” of depletion potentials: the well-depth is typically proportional to the osmotic pressure of the small particles while the range is related to their diameters, leading to rich and interesting experimental phenomena (see e.g. Crocker *et al.* 1999; Poon *et al.* 1999; Rudhart *et al.* 1998; Verma *et al.* 1998). To study this further, consider a binary HS mixture of large (species 1) and small (species 2) spheres. The complete description of a binary hard-sphere model demands not only the specification of two hard-sphere diameters,  $\sigma_1$  and  $\sigma_2$ , but also the specification of the cross-diameter  $\sigma_{12}$  denoting the distance of closest approach between two dissimilar spheres. This is traditionally written as:

$$\sigma_{12} = \frac{1}{2}(\sigma_1 + \sigma_2)(1 + \Delta) \quad (3.1)$$

When  $\Delta = 0$ , the cross-diameter is simply the sum of the two radii, exactly what one would expect on purely geometric grounds; the model is termed *additive*, and follows the traditional Lorentz mixing rule (Hansen & McDonald 1986). In nature,

however, systems will rarely be exactly Lorentz additive, and in fact positive ( $\Delta > 0$ ) or negative ( $\Delta < 0$ ) *non-additivity* will be the rule rather than the exception. This is further illustrated in figure 1. Each large particle excludes a volume  $v = \pi\sigma_{12}^3/6$  from the small particles. When two large particles approach to a distance less than  $2\sigma_{12}$ , some of this volume is doubly excluded, and the small particles can gain free-volume, and therefore entropy. Integrating out the small particles translates this entropy gain into an interaction between the large particles, the so-called depletion potential. If  $2h > \sigma_2$ , i.e. the effective exclusion diameter of small particles near a large particle is larger than their mutual exclusion diameters, then  $\Delta > 0$  and the system displays positive non-additivity. Conversely, if  $2h < \sigma_2$  then  $\Delta < 0$  and the system displays negative non-additivity. Experimental systems which display negative non-additivity include sterically or electrostatically stabilized binary colloid mixtures (Louis *et al.* 2000a). Polymer-colloid mixtures typically show positive non-additivity, and in the extreme limit,  $\sigma_2 \rightarrow 0$  with  $h$  finite, the depletion potential ( $w^{(2)}(R_{ij})$  of the appendix) reduces to the Asakura-Oosawa form (Asakura & Oosawa 1958, Vrij 1976):

$$\beta V_{AO}(r) = -\rho_2 \frac{4\pi}{3} (\sigma_{12})^3 \left\{ 1 - \frac{3}{4} \frac{r}{\sigma_{12}} + \frac{1}{16} \left( \frac{r}{\sigma_{12}} \right)^3 \right\} \quad (3.2)$$

in the range  $\sigma_1 < r \leq 2\sigma_{12}$ ; here  $\rho_2 = N_2/V$ . The value at contact is given by:

$$\beta V_{AO}(r = \sigma_1) = -\rho_2 \frac{\pi}{4} \left( \sigma_1 (2h)^2 + \frac{2}{3} (2h)^3 \right), \quad (3.3)$$

which does not depend explicitly on the small particle diameter  $\sigma_2$  or the packing fraction  $\eta_2$ .

For finite  $\sigma_2$  the effective pair potentials reduce to (3.2) and (3.3) only in the  $\rho_2 \rightarrow 0$  limit. Deriving quantitatively accurate depletion potentials at finite  $\sigma_2$  and  $\rho_2$  for non-additive systems has become possible due to some important new developments (see e.g. Roth *et al.* 2000a). Briefly, the method works like this: for a given small particle fugacity  $z_2$ , the pair-contribution to the exact effective potential,  $w^{(2)}(r; z_2)$ , is given by the difference in grand potential between a system with two large-spheres at a distance  $r$ , and the same system with the two large spheres at  $r = \infty$ . Within a density functional theory (DFT) approach, this can be rewritten as:

$$\beta w^{(2)}(r; z_2) = \lim_{\rho_1 \rightarrow 0} \left( c_1^{(1)}(\infty) - c_1^{(1)}(r) \right), \quad (3.4)$$

where  $c_1^{(1)}(r) = -\beta \delta F_{ex}[\rho_1, \rho_2] / \delta \rho_1$ ,  $F_{ex}[\rho_1, \rho_2]$  being the excess intrinsic free-energy functional of the binary mixture. By employing the Rosenfeld fundamental measure theory DFT (Rosenfeld 1989), quantitatively accurate depletion potentials can be derived for both additive (Roth *et al.* 2000a) and non-additive mixtures (Roth & Evans 2001b).

The Roth DFT method extracts the effective pair-potential from the one-body correlations as shown in equation (3.4). On the other hand, direct functional differentiation of the same Rosenfeld DFT leads to two-body correlations that are equivalent to the Percus-Yevick (PY) approximation in the homogeneous limit (Rosenfeld

1989). But, as shown in the appendix, PY results in a poor representation of the effective pair potentials. Curiously, the same DFT approach provides quantitatively accurate effective potentials by one route, and rather poor potentials by another route. For this reason, some care must be taken when choosing a particular route to thermodynamics or effective potentials from a given (approximate) DFT.

The effect of non-additivity on the depletion potentials is shown in figure 2(a), where the parameters are chosen such that  $\rho_2 h^3$  is kept constant, but  $\sigma_2$  is varied. Note in particular that for positive non-additivity ( $\sigma_2 < 2h$ ) the contact value changes very little. In contrast, for negative non-additivity ( $\sigma_2 > 2h$ ), the contact value increases markedly and can even become positive. The non-additivity can also be varied by keeping the small-particle diameter  $\sigma_2$  and the packing fraction  $\eta_2 = \pi\rho_2\sigma_2^3/6$  fixed, as shown in figure 2(b). For positive and negative non-additivity, the oscillations due to the solvation shells remain more or less the same, but the well depth changes markedly. These trends can be understood even at the very simple level of equation (3.3), valid only as  $\rho \rightarrow 0$ , since changing  $\Delta$  while keeping  $\sigma_2$  fixed corresponds to changing  $h$  and therefore the contact value.

Non-additivity has an even more dramatic effect on the virial coefficients. The additive case seems to be marginal since a very small negative or positive non-additivity markedly changes the behaviour of  $B_2$  away from the additive value (Louis & Roth 2000e). A connection to phase behaviour can be made through the recent observation of Vliegthart and Lekkerkerker (2000), who showed that  $B_2/B_2^{HS} \approx -1.5$  near the critical point of a wide variety of fluid systems. The large effect of non-additivity on the virial coefficients found by Louis and Roth (2000e) can therefore rationalize the large effect of non-additivity found in previous direct studies of the fluid-fluid spinodal line (Biben & Hansen 1997, Dijkstra 1998, Louis *et al.* 2000a). Positive non-additivity strongly favours phase-separation, while even a very small negative non-additivity has the opposite effect.

More realistic two-component systems include attractive or repulsive potentials  $v_{ij}(r)$  in addition to the hard-core steric repulsion. These can be mapped onto the non-additivity in the following way: An attractive cross-term  $v_{12}(r)$  or a repulsive small-small interaction  $v_{22}(r)$  corresponds to  $\Delta > 0$ , while a repulsive  $v_{12}(r)$  or attractive  $v_{22}(r)$  lead to  $\Delta < 0$ . In this way the large-small or small-small interactions can be used to “engineer” a very wide variety of effective potential shapes and associated fluid behaviours (Louis & Roth 2000e).

### (b) Energetic fluids: Structure and thermodynamics

#### (i) Thermodynamics

Effective depletion potentials can have a much shorter range than the hard-core diameter of the larger colloidal species. This leads to perhaps the best-known breakdown of the simple atomic fluid analogy, namely the metastability of the fluid-fluid transition w.r.t. the fluid-solid transition for short-range potentials (Gast *et al.* 1983; Hagen & Frenkel 1994). As demonstrated in figure 3, this leads to crystallization at much smaller large-sphere packing fractions than found for the archetypical freezing transition in one-component HS fluids. The relative insensitivity of the crystallization line to the form and range of the potentials shown in figure 3 is particularly striking. The determining factor is mainly the depth of the attractive well at  $r = r_{min}$ , from which, for the range of potentials probed here, an approxi-

mate crystallization criterion can be derived (Louis *et al.* 2000a): the liquidus line broadens to about 50% of the packing fraction at freezing for pure HS's when  $\beta V_{eff}(r_{min}) \approx 2.4 \pm 0.3$ †

The insensitivity of crystallization to the potential range can be understood from the trends in the free-energy curve. With increasing well-depth, the fluid branch of the free-energy in figure 4 is only mildly affected, while the solid branch develops a deep minimum, driven by close contact of the potential wells at a very high packing fraction‡. Equilibrium between a very dense solid and a dilute fluid can now easily be achieved. (This can be seen in figure 4 by using the common tangent construction.) ‡. Therefore, when the liquidus line broadens, crystallization is driven primarily by changes in the close-packed solid branch of the free energy, which probes well depths at the potential minima, but is largely independent of other features of the potentials. This is the origin of the semi-universal crystallization law found by Louis *et al.* (2000a).

## (ii) Structure

In the regime where the crystallization curve broadens to lower and lower packing fractions of the large-particles, the structure can be well approximated by the very simple form:  $g(r) = \exp[-\beta w^{(2)}(r; z_2)]$  (Louis 2000b), where  $w^{(2)}(r; z_2)$  is the two-body contribution of the exact effective potential (EEP) described in the appendix. As demonstrated in figure 5, this works remarkably well, even for densities as high as  $\eta_1 = 0.25$ . Because the fluid-fluid transition is metastable and crystallization typically sets in only for a well-depth of order  $\beta V(r_{min}) \approx 2.4$ , the  $g(r)$  near contact can easily approach values greater than 10 in the fluid phase, which is quite different from the value for a HS reference system at the same overall density.

If experiments could directly access  $g(r)$ , this would lead to a very simple method to extract the effective potentials. However, experiments on pair-correlations typically access  $S(k)$ , where the effect of the potentials is much less clear cut, as demonstrated in figure 6. In contrast to the van der Waals picture, the effective potentials alter the  $S(k)$  quite markedly from the HS reference system, but similarly to the van der Waals picture, where deriving the attractive contribution to the potential from an inversion of  $S(k)$  is very difficult (Reatto 1986), quite a number of different effective potentials may result in similar behaviour for  $S(k)$ . The potentials in figure 6 were chosen to have nearly equal virial coefficients  $B_2$ . Since  $2B_2 = -\hat{f}(0)$ , where  $\hat{f}(k)$  is the Fourier transform (FT) of the Mayer function  $f(r) = \exp[\beta v(r)] - 1$ , (which in turn provides a good approximation for the total correlation function

† As the potential becomes more short-ranged, the trend is towards somewhat higher values of  $\beta V_{eff}(r_{min})$ . Nevertheless, this very simple criterion describes the dominant effect in the range of most interest to experiment.

‡ This well in the crystal free-energy branch also drives the solid-solid transition

‡ While the solid must be treated accurately, small errors in the fluid-free energy have little effect on the fluid-solid transition in the energetic fluid regime, in marked contrast to the pure HS case where both branches of the free energy must be treated accurately. The free-energies in figure 4 were generated with first order thermodynamic perturbation theory. They reproduce the fluid-solid phase-behaviour of short-range potentials rather well, but fail miserably for the (metastable) fluid-fluid transition (Dijkstra *et al.* 1999b, Louis 2000a). First order perturbation theory even fails to correctly describe the second virial coefficient, so it is not surprising that it breaks down for the fluid-fluid line.

$h(r) = g(r) - 1$  in this regime) it is not surprising that  $S(k) = 1 + \rho \hat{h}(k)$  should be similar for different potentials as long as  $B_2$  is held constant.¶

The fluid-solid transition is mainly determined by the potential minimum, and is therefore not directly related to  $B_2$  (compare, for example, the virial-coefficients of the potentials depicted in the inset of figure 3). This implies that  $S(k)$ , which is mainly determined by  $B_2$ , will vary significantly for different potentials along the fluid-solid line. Therefore the Hansen-Verlet criterion, or any other similar criterion based on  $S(k)$ , will not hold in this “energetic fluid” regime.

(iii) *The energetic fluid picture vs. the van der Waals picture of fluids*

The term *energetic fluid* applies to the fluid phase at low overall packing fraction of the large-particles (say  $\eta \leq 0.25$ ), as shown schematically in figure 3. This regime opens up in short-range potential fluids when the fluid-fluid phase-line becomes metastable to the fluid-solid line, which then broadens out to very low packing fractions. While it is hard to find atomic or molecular fluids with a potential range short enough to qualify for this nomenclature, many solutes in solution are governed by relatively short-range attractive potentials. Through McMillan-Mayer solution theory (McMillan and Mayer 1945) they can be viewed as effective atomic fluids. But in contrast to the van der Waals picture described in section 2, the attractive potentials of such energetic fluids qualitatively affect both freezing and structure:

- **Freezing:** The liquidus line is determined primarily by the well-depth of the potential, and less so by other details such as its range or shape. While in the van der Waals picture freezing is driven by entropic excluded volume effects, here it is driven by (energetic) properties of the potentials.
- **Structure:** The real-space structure of energetic fluids can be qualitatively described by the simple relation  $g(r) = \exp[-\beta v(r)]$ , while the k-space structure  $S(k)$  is well described by the Baxter model at the same  $B_2$ . In contrast, the  $S(k)$  of van der Waals fluids typically resembles that of a HS fluid.

is mainly determined by the value of the second virial coefficient rather than by other details of the potentials.

Examples of energetic fluids include many colloidal suspensions, where direct interactions can be of short range, or else where other (smaller) colloids, micelles, or polymers can act as depletants, inducing potentials such as those depicted in figure 2.

Globular proteins may also fall into the same class, but their interactions are no longer spherically symmetric (Durbin & Feher 1996; Lomakin *et al.* 1998; Neal *et al.* 1998; Piazza 2000; Sear 1999). The radial distribution function and structure factor should still display behaviour similar to other energetic fluids, but now with an implicit orientational average over the anisotropic potentials.

Proteins typically crystallize at very low packing fractions, and some show evidence of a phase diagram topology similar to the one depicted in figure 3 (Frenkel 2000; Piazza 2000; Rosenbaum 1996; Sear 1999), with a metastable fluid-fluid line. There is also evidence that potential contacts in the crystal are very important

¶ This simple picture breaks down near the spinodal line where  $S(k = 0)$  is enhanced by collective density fluctuations.

for protein crystallization (Durbin & Feher 1996), which is consistent with energetic fluid behaviour and in sharp contrast to what would be expected from the van der Waals picture. The semi-universality of crystallization found for spherically symmetric potentials depends on similar behaviour of the solid branch of the free-energy for different potential shapes. Unfortunately, this can no longer be expected for proteins, since (a) the proteins are no longer spherical and (b) the potentials are anisotropic (or “patchy”), leading to many possible crystal structures. In fact, as emphasized by Sear (1999), conditions (a) and (b) suggest that some proteins may be very difficult to crystallize precisely because their potential contacts are not commensurate with an allowed crystal structure. So, whether globular proteins can be usefully classified as energetic fluids remains to be seen, but they can certainly not be classified within the van der Waals picture of fluids.

#### 4. Example B: Polymers as soft colloids: Mean field fluids

##### (a) Deriving effective polymer-polymer potentials

The approach outlined here, described in more detail in (Louis *et al.* 2000c, Bolhuis *et al.* 2001), is to coarse-grain the polymers by integrating out monomeric degrees of freedom, resulting in a description based on the polymer centres of mass (CM). In principle, for a set of  $N_1$  polymers with  $L$  monomers each, one could calculate the EEP which depends explicitly on the configuration  $\{R_i\}$  of the centres of mass. The only differences with the binary-mixture case described in the appendix are: (1) there is no explicit additional dependence on the monomer density (or fugacity), since that is fixed by the number of polymers in the set  $\{R_i\}$ , and (2) there is no *direct* interaction  $V(\{R_i\})$ ; the polymer-polymer effective potential arises solely from the coarse-graining procedure. The EEP now takes the form:

$$W^{eff}(\{R_i\}) = \sum_{i<j}^{N_1} w^{(2)}(R_{ij}) + \sum_{i<j<k}^{N_1} w^{(3)}(R_{ijk}) + \dots, \quad (4.1)$$

and again, each term could in principle be calculated separately, but this rapidly becomes intractable. Instead, one can follow the second route described in the appendix and include all higher order terms in equation (4.1) through the density dependence of an effective pair potential  $w(r; \rho_1)$ , which exactly reproduces the CM pair-correlations at a given density  $\rho_1 = N_1/V$ . To do so, we first perform Monte Carlo (MC) simulations of self avoiding walk  $L = 500$  chains on a simple cubic lattice and extract the radial-distribution functions  $g(r)$  between the CM. These are then inverted through an Ornstein-Zernike procedure using the hypernetted-chain closure (HNC), which has been shown to be quasi-exact for the potentials under consideration (Louis *et al.* 2000b, 2000d, Bolhuis *et al.* 2001). Figure 7 shows both the radial-distribution functions and the effective potentials inverted from the  $g(r)$ . According to the theorems discussed in the appendix, the effective-potentials should, through the pair-correlations and equation (A 9), reproduce the contributions to the (osmotic) compressibility induced by the EEP (4.1). Figure 8 shows that the total compressibility is very well approximated in this approach, implying that, in contrast to the binary fluid case, the volume term contribution (defined in the appendix) is small. The difference in volume terms is most likely due to the

fact that the number of monomers is fixed by the number of polymers, instead of being free to vary as is the case for the small particles in the binary mixture. In fact, if the polymers were rigid, their CM correlations would exactly determine the compressibility (see e.g. Hansen & McDonald 1986 ch 12).

(b) *Mean Field Fluids: structure and thermodynamics*

The effective potentials shown in figure 7 are radically different from the usual hard-core plus attraction form found for atomic systems, immediately suggesting different fluid behaviour. Already the radial distribution functions in figure 7 appear to be quite different from their atomic-fluid counterparts. The structure of fluids described by these potentials is well approximated by the simple random phase approximation over a surprisingly large density range (Louis *et al.* 2000*d*, Likos *et al.* 2000). Marked differences with atomic fluid behaviour also arise at the level of thermodynamics, where the equation of state (EOS) is very well described by the following mean-field form:

$$Z = \frac{\beta P}{\rho} \approx Z_{MF} = 1 + \frac{1}{2}\rho \int d\mathbf{r} \beta v(r) = 1 + \frac{1}{2}\beta \hat{v}(k=0)\rho \quad (4.2)$$

As shown in figure 9, this also holds for integrable potentials which diverge at the origin. Equation (4.2) demonstrates that what matters is the value of the FT of the potential at the origin,  $\beta \hat{v}(k=0)$ , which is finite for all 3 potentials, and, in figure 9, chosen to have the same value to ensure that the three EOS are very close. The quasi-linear behaviour of the EOS resembles that of an atomic fluid in the second virial approximation, but, in fact, the three potentials have virial coefficients differing by about 10%. More seriously, the virial expansion has a surprisingly small radius of convergence so that adding higher order virial coefficients results in a much poorer approximation (Louis *et al.* 2000*d*), as demonstrated by the third order virial expansions in figure 9.

Instead of the CM, end-points or mid-points could also be used to construct an effective particle picture of interacting polymer solutions. For example, the mid-point representation would be very similar to the two-arm limit of a star-polymer, for which a number of results have been recently derived (Likos *et al.* 1998; Likos 2001; Watzlawek *et al.* 1999). In figure 10 the  $f = 2$  limit of the star-polymer potential is compared to a more recent expression for the mid-point–mid-point interaction (Dzubiella *et al.* 2000). At first sight the two appear very similar, but the slope of their respective EOS differ by a factor of four! The reason for this can be seen in figure 11: Since  $\beta \hat{v}(k=0)$  is proportional to the integral over  $r^2 \beta v(r)$ , it is the small differences (much less than  $k_B T$ ) in the tails of the two  $\beta v(r)$  that determine the large differences in the EOS. Interestingly the two radial-distribution functions are again quite similar (although the associated structure factors are not).

(c) *Mean field fluids vs. the van der Waals picture of fluids*

A necessary, but not sufficient condition for mean field fluid (MFF) behaviour is that  $\beta \hat{v}(k=0)$  is finite. If  $\beta \hat{v}(k=0)$  is relatively large, then MFF behaviour, with its quasi-linear EOS and correlation functions well-described by the random phase approximation, only sets in for large enough densities. At lower densities the

structure can still resemble that of a HS fluid, but the topology of the phase-diagram is quite different (Lang *et al.* 2000, Louis *et al.* 2000*d*). Depending on whether the FT of the potential oscillates or not, such fluids may show either re-entrant melting or else a clustering transition for large enough values of  $\beta\hat{v}(k=0)$  (Likos *et al.* 2000).

Systems with values of  $\beta\hat{v}(k=0)$  significantly below the value that can induce freezing or clustering transitions are MFF at all densities. The associated simple equation of state and fluid-structure are markedly different from the behaviour of fluids in the van der Waals picture†.

## 5. Conclusions

While the van der Waals picture of fluids lies at the basis of many successful liquid state theories for atomic and molecular fluids, it breaks down for the richer class of potentials arising from coarse-graining procedures in complex fluids. Nevertheless, a judicious choice of techniques drawn from the theory of simple liquids may still provide insight when combined with a careful derivation of effective potentials. Some recent examples of this programme include the phase-diagram of additive (Dijkstra *et al.* 1999*a*) and non-additive (Louis *et al.* 2000*a*) asymmetric binary HS mixtures, the structure and phase-behaviour of star-polymers (Likos *et al.* 1998; Watzlawek *et al.* 1999), and star-polymer colloid mixtures (Dzubiella *et al.* 2000), and the structure and phase-behaviour of a pure-polymer system (Louis *et al.* 2000*c*; Bolhuis *et al.* 2001). In each case the effective potential picture was the key to clarifying the underlying physics.

Similarly, in this contribution a derivation of the effective potentials in binary hard-sphere fluids demonstrated the key role of non-additivity in determining the shape of the effective depletion potentials, and the associated phase behaviour. When such potentials are short ranged, they open up a region in the phase-diagram where the fluid behaviour deviates significantly from the van der Waals picture, so much so in fact, that a new nomenclature, *energetic fluids*, has been introduced. In the energetic fluid regime, the structure can be described by a very simple form: in real space  $g(r) = \exp[-\beta w^{(2)}(r; \rho_2)]$ , while in reciprocal space  $S(k)$  is largely determined by the virial coefficient  $B_2$ . For a wide variety of potential shapes, the liquidus line broadens to low large-particle densities when well-depth  $\beta w^{(2)}(r_{min}; \rho_2) \approx 2.4$ .

When linear or star polymers in solution are represented as “soft colloids” centred around their mid-points or their CM, the resultant picture leads to effective potentials with a finite value of  $\beta\hat{v}(k=0)$ . Again, such fluids do not follow the van der Waals picture. For example, their EOS closely follows a mean-field linear form  $\beta P/\rho \approx 1 + 1/2\rho\beta\hat{v}(k=0)$ , and their structure is well described by the simple random phase approximation closure: behaviour best classified under the moniker *mean field fluids*.

Most of this work was done in close collaboration with J.P. Hansen, P.G. Bolhuis, R. Roth, R. Finken, and E.J. Meijer, and has appeared in our joint publications listed in the references. I thank David Rowan for a critical reading of the manuscript and gratefully acknowledge financial support from the Isaac Newton Trust, Cambridge.

† Perhaps I’m beating a straw man here, but the distinctions are hopefully helpful nonetheless

## Appendix A. Two ways of deriving effective potentials for binary mixtures

Consider a binary mixture of large (species 1) and small (species 2) spherical particles. Integrating out the smaller component to derive a new one-component fluid interacting through effective depletion interactions is a useful way to treat such systems. This appendix will focus on two popular ways to derive these effective potentials:

### (i) Method 1: Exact effective potential

For binary mixtures the exact effective potential (EEP) is most easily analyzed in the semi-grand ensemble, where the number of large particles  $N_1$  and the fugacity  $z_2$  of the small particles is fixed (Lekkerkerker *et al.* 1992, McMillan & Mayer 1945)†. Given a set of  $N_1$  large particles fixed at positions  $\{R_i\}$  in a volume  $V$ , the small particles are integrated out by calculating their partition function in the fixed external field generated by the large particles. This results in an effective grand potential for the small particles of the form:

$$\Omega(N_1, z_2, V; \{R_i\}), \quad (\text{A } 1)$$

which depends parametrically on the large-particle positions  $\{R_i\}$ ‡. To make further progress we follow the analysis of Dijkstra *et al.* (1999a, 1999b, 2000), and decompose this grand potential into n-body terms. Using this mapping, a one-component system can be derived with an an effective interaction of the form:

$$v_{11}(\{R_i\}) + \Omega(N_1, z_2, V; \{R_i\}) = V^{(0)}(N_1, z_2, V) + W^{eff}(\{R_i\}; z_2), \quad (\text{A } 2)$$

where  $v_{11}(\{R_i\})$  is the direct interaction between the large spheres that is already present in the original two component system,  $V^{(0)}(N_1, z_2, V)$  is the so-called volume term (which depends on the set  $\{R_i\}$  only through the total number of large particles  $N_1$ , but is independent of their relative positions)¶, and  $W^{eff}(\{R_i\}; z_2)$  is the EEP which can be further expanded as:

$$W^{eff}(\{R_i\}; z_2) = \sum_{i < j}^{N_1} \left( v_{11}^{(2)}(R_{ij}) + w^{(2)}(R_{ij}; z_2) \right) + \sum_{i < j < k}^{N_1} \left( v_{11}^{(3)}(R_{ijk}) + w^{(3)}(R_{ijk}; z_2) \right) + \dots \quad (\text{A } 3)$$

The pair term is simply the sum of the pair contribution to the direct interaction,  $v_{11}^{(2)}(R_{ij})$ , and the effective interaction  $w^{(2)}(R_{ij}; z_2)$  induced by integrating out the small spheres. It is precisely this pair term which is measured in the laser tweezer experiments (Verma *et al.* 1998, Crocker *et al.* 1999). The triplet term is a similar sum of direct and induced terms with  $R_{ijk}$  the standard 3-body coordinates and

† Charged systems are best analyzed in the the canonical ensemble. An early example would be the effective potentials in liquid metals (Ashcroft & Stroud 1978)

‡ Explicit temperature dependence is omitted in this section

¶ For binary fluids the volume term is given by:  $V^{(0)}(N_1, z_2, V) = -p_2(z_2)V + N_1 w^{(1)}(z_2)$  where  $p_2$  is the pressure of a pure component 2 system at fugacity  $z_2$ , and  $w^{(1)}(z_2)$  is the grand potential difference due to adding one large component 1 particle to the same system. One body terms which depend on the configuration  $\{R_i\}$  are zero due to translational invariance.

so forth for n-body interactions. (Since the individual terms  $w^{(n)}(R_{ij\dots})$  depend only on the large-small and small-small interactions, their form is independent of  $v_{11}(\{R_i\})$ , which need not be decomposable as a sum of pair terms.) The induced pair term can be rigorously defined as the difference between the grand potential of equation (A 1) for two particles a distance  $R_{ij} = |\mathbf{R}_i - \mathbf{R}_j|$  apart, and the grand potential when the two particles are an infinite distance apart. From (A 3) this reduces to  $w^{(2)}(R_{ij}; z_2) = \Omega(N_1 = 2, z_2, V; R_{ij}) - V^{(0)}(N_1 = 2, z_2, V)$ . Similarly the induced three-body potential can be defined as:

$$\begin{aligned} w^{(3)}(R_{ijk}; z_2) &= \Omega(N_1 = 3, z_2, V; R_{ijk}) - V^{(0)}(N_1 = 3, z_2, V) \\ &- w^{(2)}(R_{ij}; z_2) - w^{(2)}(R_{ik}; z_2) - w^{(2)}(R_{jk}; z_2), \end{aligned} \quad (\text{A } 4)$$

i.e. it is that part of the interaction induced by 3 large spheres which cannot be described by volume and pair interaction terms alone. By continuing in similar fashion for higher and higher order terms the full EEP can be built up such that the exact free energy of the mixture is given by:

$$F(N_1, z_2, V) = V^{(0)}(N_1, z_2, V) + F^{eff}(N_1, z_2, V), \quad (\text{A } 5)$$

where  $F^{eff}(N_1, z_2, V)$  is defined as the free energy of a one-component system interacting through the EEP, i.e.  $\exp[-\beta F^{eff}] = Tr_1 \exp[-\beta W^{eff}]$ . In other words, by exactly integrating out the small particles for an arbitrary configuration  $\{R_i\}$ , the original two-component partition sum has been rewritten as a weighted sum over large particle configurations only. The EEP describes the weighting of each individual large-particle configuration in the effective one-component partition sum, while the volume term adds the left over contributions independent of the large-particle configurations.

Calculating the EEP to all orders is usually impractical. Instead what is often done is to truncate the series (A 3) and retain only the pair potential. In many cases this is not such a bad approximation, and for a few systems it is even exact. For example, the EEP for the Asakura Oosawa (AO) model (Asakura & Oosawa 1958, Vrij 1976) with size-ratio  $q = \sigma_2/\sigma_1 < 2/\sqrt{3} - 1 \simeq 0.1547$  is exactly described by the pair term<sup>†</sup>. Similarly, for  $0.1547 < q < \sqrt{3/2} - 1 \simeq 0.2247$  the EEP is exactly described by the pair term and a triplet term. But even for this rather simple model, the exact form of  $w^{(3)}(R_{ijk}; z_2)$  is very tedious to calculate (Goulding 2000). Thankfully, simulations have shown that neglecting the higher order terms for the AO model often works admirably well even for size ratios as large as  $q = 0.5$ , (Meijer & Frenkel 1994; Dijkstra *et al.* 1999a, 1999b).

## (ii) Method 2: Inverting the pair correlations

The correlations functions in an effective one-component system interacting through the full EEP (A 3) are equal to the correlation functions between the large particles in the original two-component system, as long as both are at the same state point (see e.g. Dijkstra *et al.* 2000)<sup>‡</sup>. For example,  $S(k) = S_{11}(k)$ , where the

<sup>†</sup> Another even simpler example with only a pair term is the exactly solvable lattice model of Frenkel and Louis (1992).

<sup>‡</sup> The volume terms do not directly contribute to the pair and higher order correlations although they may contribute indirectly through changing the phase-behaviour of the system. For

first structure factor is that of the effective one-component system and the second is that of the original two-component system. This equivalence also implies that

$$\lim_{\rho_1 \rightarrow 0} g_{11}(r; z_2) = \exp \left[ -\beta \left( v_{11}^{(2)}(r) + w^{(2)}(r; z_2) \right) \right], \quad (\text{A } 6)$$

where  $g_{11}(r; z_2)$  is the radial distribution function of the large-spheres. †. Similar expressions can be derived to link higher order correlation functions to higher order terms in the EEP (A 3). Hence, there is a *direct link* between the EEP of the effective one-component system and the  $\rho_1 \rightarrow 0$  limit of the fluid correlation functions in the homogeneous phase of the original two-component model‡

The relation (A 6) may be generalized to finite densities of species 1, because there exists a one-to-one mapping:

$$g(r; \rho) \leftrightarrow w(r; \rho) \quad (\text{A } 7)$$

between a given pair distribution function  $g(r)$  at density  $\rho$  and a *unique* two-body pair potential  $w(r; \rho)$  which reproduces  $g(r)$  *irrespective of the underlying many-body interactions* in the system (Henderson 1974; Chayes *et al.* 1984). Since at finite densities the radial distribution function  $g(r; \rho_1, z_2) = g_{11}(r; \rho_1, z_2)$  includes contributions not only from the pair-interactions, but also from higher order contributions to  $W^{eff}(r; z_2, \{R_i\})$ , the effective pair-potential includes these terms in an averaged way. It can be written as:

$$w(r; \rho_1, z_2) = v_{11}(r) + \tilde{w}(r; \rho_1, z_2) \quad (\text{A } 8)$$

which is connected to equation (A 6) through  $\lim_{\rho_1 \rightarrow 0} \tilde{w}(r; \rho_1, z_2) = w^{(2)}(r; z_2)$ .

The price paid for including the effect of all higher order terms is to introduce a density dependence in the pair-potential, but the payoff is that the pair-correlations are exactly reproduced (but not the triplet or higher order correlations). Thermodynamics can then be extracted through the compressibility relation:

$$\left( \frac{\partial \beta \Pi_1}{\partial \rho_1} \right)_{N, z_2} = \lim_{k \rightarrow 0} \frac{1}{S(k)}. \quad (\text{A } 9)$$

Note, however, that volume terms can also contribute to the total EOS (Dijkstra *et al.* 2000), so that equation (A 9) describes the osmotic compressibility due to species 1 only. In some cases this is only a small fraction of the total compressibility of the full two-component system (Louis *et al.* 1999; Dijkstra *et al.* 2000).

How does one perform the  $g(r; \rho) \leftrightarrow w(r; \rho)$  inversion? If the full EEP includes only pair terms (as is the case for the AO model with  $q < 0.1547$ ), then  $w(r; \rho_1, z_2) =$

the binary mixtures considered here they don't affect phase-boundaries (Dijkstra *et al.* 1999a), but for other systems they can (van Roij & Hansen 1997; van Roij *et al.* 1999; Graf & Löwen 1998; Warren 2000), and so must be taken into account to correctly describe the equivalent state points of the original two-component and effective one-component systems

† Most information about  $g_{12}(k)$  and  $g_{22}(k)$  is lost in the mapping.

‡ Note that equation A 6 is different from the potential of mean force which is typically defined as  $\beta w^{pmf}(r) = -\ln[g(r)]$  for any density and is strictly speaking not a pair potential, but a restatement of the pair-distribution function. For example, a system directly interacting through a  $\beta w^{pmf}(r)$  derived at finite  $\rho$  will not have the same correlations as the original system from which the potential of mean force was derived.

$w^{(2)}(r, z_2)$  at all densities. If it only includes pair and triplet terms (as for the AO model with  $0.1547 \leq q \leq 0.2247$ ) then to a good approximation (Reatto & Tau 1987; Attard 1992):

$$w(r_{12}; \rho_1, z_2) \approx w^{(2)}(r_{12}; z_2) - \rho_1 \int d\mathbf{r}_3 \left[ e^{-w^{(3)}(\mathbf{r}_1, \mathbf{r}_2, \mathbf{r}_3; z_2)} - 1 \right] g(r_{13})g(r_{23}). \quad (\text{A } 10)$$

More generally, one needs (i) a method to generate the exact  $g_{11}(r)$  for the two component system and (ii) an inversion method to extract  $\beta v(r)$  from  $g(r)$ . Inversion methods based on the Ornstein-Zernike relations exist (Reatto 1986, Zerah and Hansen 1986), but these are very sensitive to the underlying approximations and the quality of the original pair-correlations used as input.

As an example of the difficulties involved in (i), consider the popular Percus Yevick (PY) approximation which is exactly soluble for binary HS mixtures (Lebowitz & Rowlinson 1965). On the one hand PY approximates the EOS very well, but on the other hand the PY approximation to the large-particle correlation function in the  $\rho_1, \rho_2 \rightarrow 0$  limit reduces to:

$$\lim_{\rho_1, \rho_2 \rightarrow 0} g_{11}^{PY}(r) = 1 - \beta V_{AO}(r) \quad (\text{A } 11)$$

instead of the correct exponential form:  $\exp[-\beta V_{AO}(r)]$  (note that  $w^{(2)}(r; \rho_2) = V_{AO}(r)$  in this limit). For finite  $\rho_2$ ,  $w^{(2)}(r; \rho_2)$  begins to deviate from the AO form, but PY still approximately linearizes the exponential, as illustrated in figure 12. In spite of the fact that PY successfully describes the EOS, it clearly fails quite badly for the effective potential, especially near contact<sup>†</sup>, suggesting that an inversion of PY at finite densities should also fail. More generally, using 2-component integral equations to derive effective pair potentials or phase-behaviour in the ‘‘colloidal limit’’ (small  $y$ , large  $\eta_2$  and small  $\eta_1$ ) is fraught with difficulty. For example, Biben *et al.* (1996) showed how two self-consistent closures that work extremely well for one-component systems, RY and BPGG, predict quite different locations of the fluid-fluid spinodal line in binary HS mixtures. A comparison of the effective pair potentials  $w^{(2)}(r; \rho_2)$  calculated for each closure by these authors can, in fact, rationalize the difference, since these effective potentials are what primarily determines the phase-behaviour. This suggests that for two-component integral equations in the colloidal limit, it is much better to compare the performance for the large particle osmotic pressure rather than the performance for the full EOS, which is typically dominated by the small-particle contribution.

## References

- Alder, B.J. & Wainwright, T.E. 1957 J. Chem. Phys. **27**, 1208.  
 Asakura, S. & Oosawa, F. 1954 J. Chem. Phys. **22**, 1255.  
 Asakura, S. & Oosawa, F. 1958 J. Polym. Sci. Polym. Symp. **33**, 183.  
 Ashcroft, N.W. & Lekner, J. 1966 Phys. Rev. **145**, 83.  
 Ashcroft, N.W. & Stroud, D. 1978 Solid State Physics **33** 1

<sup>†</sup> PY is reasonably accurate for the EOS because it is dominated by the small particle contributions in the  $\rho_1 \rightarrow 0$  limit.

- Attard, P. 1992 Phys. Rev. A **45**, 3659.
- Barker, J.A. & Henderson, D. 1967 J. Chem. Phys. **47**, 4714.
- Biben, T. & Hansen, J.P. 1991 Phys. Rev. Lett. **66**, 2215.
- Biben, T. & Bladon, P. & Frenkel, D. 1996 J. Phys. Condensed Matter, **8** 10799.
- Biben, T. and Hansen, J.P. 1997 Physica A **235**, 142.
- Bolhuis, P.G. & Louis, A.A. & Hansen, J.P. & Meijer, E. J. 2001 J. Chem Phys. (to appear).
- Chandler, D. & Weeks, J.D. Phys. Rev. Lett. **25**, 149 (1970); Weeks, J.D. & Chandler, D. & Andersen, H.C. 1971 J. Chem. Phys. **54**, 5237.
- Chandler, D. & Weeks, J.D. & Andersen, H.C. 1983 Science **220**, 787.
- Chayes, J.T. & Chayes, L. 1984 J. Stat. Phys. **36**, 471.
- Crocker, J.C. & Matteo, A.D. & Dinsmore A.D. & Yodh, A.G. 1999 Phys. Rev. Lett. **80**, 409
- Dijkstra M. 1998 Phys. Rev. E. **58**, 7523.
- Dijkstra, M. & van Roij, R. & Evans, R, 1999a Phys. Rev. E. **59**, 5744.
- Dijkstra, M. & Brader, J. & Evans, R, 1999b J. Phys.: Condens. Matter **11**, 10079.
- Dijkstra, M. & van Roij, R. & Evans, R, 2000 J. Chem. Phys. **113**, 4799.
- Durbin S. D. & Feher, G. 1996 Ann. Rev. Phys. Chem. **47** 171
- Dzubiella, J. & Jusufi, A. & Likos, C.N. & von Ferber, C. & Löwen, H & Stellbrink, J. & Allgaier, J. & Richter, D. & Schofield, A.B. & Smith, P.A. & Poon, W.C.K. & Pusey, P.N. 2000 preprint cond-mat/0010176.
- Frenkel, D. and Louis, A. A. 1992 Phys. Rev. Lett. **68**, 3363.
- Frenkel, D. 2000 in ed. Cates, M.E. & Evans, M.R. *Soft and Fragile Matter* London: IOP.
- Graf, H & Löwen, H. 1998 Phys. Rev. E **57**, 5744.
- Gast, A.P. & Hall, C.K. & and Russel, W.B. 1983 J. Colloid Interface Sci. **96**, 251.
- Goulding, D. 2000 PhD thesis Cambridge University.
- Hagen, M.H. & Frenkel, D. 1994 J. Chem. Phys. **101** 4093.
- Hansen, J.P. & Verlet, L. 1969 Phys. Rev. **184** 151.
- Hansen, J.P. & McDonald, I.R. 1986 *Theory of Simple Liquids*, 2nd edn. London: Academic Press.
- Henderson, R.L. 1974 Phys. Lett. A. **49**, 197.
- Lang, A. Likos, C.N. & Watzlawek, M. & Löwen, H. 2000 J. Phys.: Condens. Matter **12**, 5087.
- Lebowitz, J.L. & Rowlinson, J.S. 1964 J. Chem. Phys. **41**, 133.
- Lekkerkerker, H.N.W. & Poon, W.C.K. & Pusey, P.N. & Stroobants, A & and Warren, P.B. 1992 Europhys. Lett. **20**, 559.
- Li-In-On, F.K.R. & Vincent, B. & Waite, F.A. 1975 ACS Symp. Ser. **9**, 165.
- Likos, C.N. & Lowen, H. & Watzlawek M. & Abbas B. & Jucknischke, O. & Allgaier J. & Richter D. & 1998 Phys. Rev. Lett. **80** 4450.
- Likos, C.N. & Lang, A. Watzlawek, M. & Löwen H. 2000 preprint condmat/0007089.
- Likos, C.N. *Effective Interactions in Soft Condensed Matter Physics* 2001, Phys. Rep. (to appear).
- Lomakin, A. & Asherie, N. & Benedek, G. 1999 Proc. Natl. Acad. Sci. USA **96** 9465.
- Longuet-Higgins, H.C. & Widom, B. 1964 Mol. Phys. **8**, 549.
- Louis, A. A. & Finken, R. & Hansen, J.P. 1999 Europhys. Lett. **46**, 741.
- Louis, A.A. & Finken, R. & Hansen, J.P. 2000a Phys. Rev. E. **61** R1028.
- Louis, A.A. 2000b Phys. Rev. Lett. **84** 1840
- Louis, A.A. & P.G. Bolhuis, Hansen, J.P. & Meijer, E. J. 2000c Phys. Rev. Lett. **85** 2522.
- Louis, A.A. & P.G. Bolhuis, Hansen, J.P. 2000d Phys. Rev. E. **62**, 7961.

- Louis, A.A. & Roth, R. 2000e preprint cond-mat/0102049.
- McMillan W.G. & Mayer, J.E. 1945 J. Chem. Phys. **13**, 276.
- Meijer, E. J. & Frenkel, D. 1994 J. Chem. Phys. **100**, 6873.
- Neal, B.L. & Asthagiri, D. & Lenhoff, A.M. 1998 Biophys. J. **75** 2469.
- Piazza R. 2000 Curr. Opin. Colloid. In. **5** 38.
- Poon, W.C.K. Renth F. & Evans R.M.L. & Fairhurst D.J. & Cates M.E. & Pusey P.N. 1999 Phys. Rev. Lett. **83**, 3960.
- Reatto, L. 1986 Phil. Mag. A **58**, 37.
- Reatto, L. & Tau, M. 1987, J. Chem. Phys. **86**, 6474.
- van Roij, R. & Hansen, J.P. 1997 Phys. Rev. Lett. **79**, 3082.
- van Roij, R. & Dijkstra, M. & Hansen, J.P. 1999 Phys. Rev. E **59**, 2010.
- Rosenbaum, D. & Zamora, P.C. & Zukoski, 1996 C.F. Phys. Rev. Lett. **77** 4832.
- Rosenfeld, Y. Phys. Rev. Lett. 1989 **63** 980.
- Roth, R. & Evans, R. & Dietrich, S. 2000a Phys. Rev. E. **62** 5360.
- Roth, R. & Evans, R. 2001b Europhys. Lett. **53**, 271.
- Rudhardt, D. & Bechinger, C. & Leiderer P. 1998 Phys. Rev. Lett. **81** 1330.
- Sear, R.P. 1999 J. Chem. Phys. **111** 4800.
- Vliegthart, G.A. & Lodge, J.F.M. & Lekkerkerker, H.N.W. 1999 Physica A 269 378.
- Vliegthart, G. A. & Lekkerkerker, H.N.W. 2000 J. Chem. Phys. **112**, 5364
- Vrij, A. 1976 Pure Appl. Chem. **48**, 471.
- Verlet, L. 1967 Phys. Rev. **165**, 201.
- Verma, R. & Crocker, J.C. & Lubensky, T.C. & Yodh, A.G. 1998 Phys. Rev. Lett. **81**, 4004.
- Warren, P J. 2000 Chem. Phys. **112** 4683
- Watzlawek, M. & Likos, C.N. & Löwen, H. 1999 Phys. Rev. Lett. **82**, 5289.
- Weeks, J.D. & Chandler, D. & Andersen, H.C. 1971 J. Chem. Phys. **54**, 5237.
- Widom, B (1967) Science **157**, 375.
- Wood, W.W. & Jacobson, J.D. 1957 J. Chem. Phys. **27** 1207.
- Zerah, G. & Hansen, J.P. 1986 J. Chem. Phys. **84** 2336.

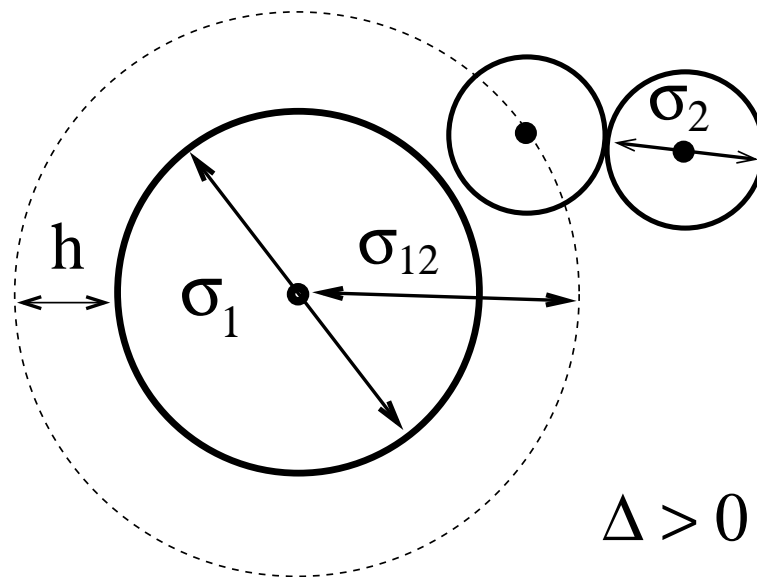


Figure 1. The centres of the small spheres can only approach to within a distance  $h = \sigma_{12} - \sigma_1/2 = \frac{1}{2}\sigma_1(\Delta + y + \Delta y)$  from the surface of the large spheres ( $y = \sigma_2/\sigma_1$ ). For an additive system  $\sigma_2 = h$ , but here  $\sigma_2 < h$  so that the system exhibits positive non-additivity.

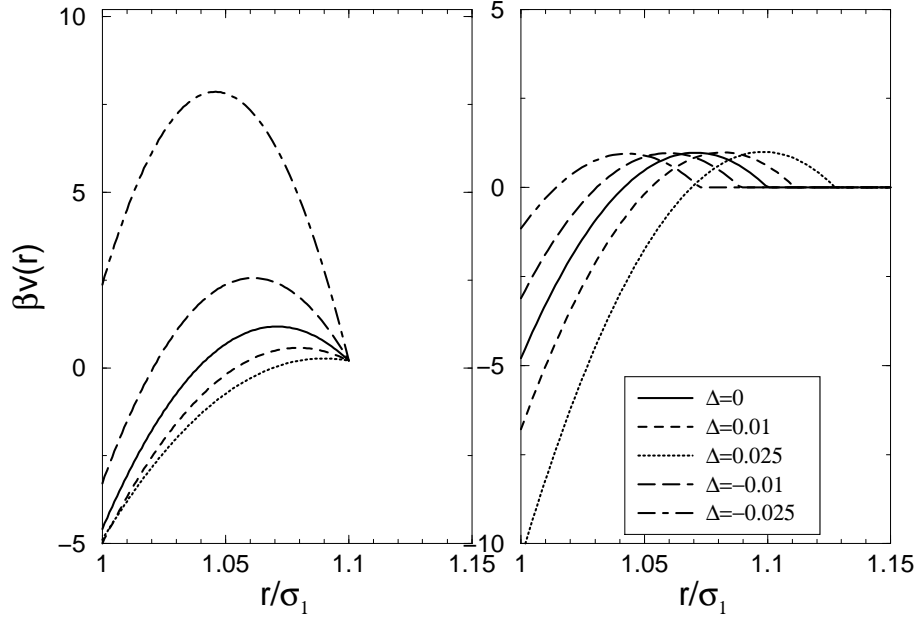


Figure 2. The effect of non-additivity on depletion pair potentials at a size-ratio  $y = \sigma_2/\sigma_1 = 0.1$ . In plot (a) the effective packing fraction  $\eta_2^{eff} = 4/3\pi\rho_2 h^3 = 0.258045$  is kept constant, while in plot (b) the small-particle packing fraction  $\eta_2 = \pi/6\rho_2\sigma_2^3 = 0.258045$  is kept constant. For the AO potential at  $y = 0.1$ , this packing corresponds to a second virial coefficient  $B_2/B_2^{HS} = -1.5$ , which is near the (metastable) fluid-fluid critical point (Vliegthart & Lekkerkerker 2000). The potentials are from Louis *et al.* (2000a), and ignore oscillations at a range  $r > 2h$ . Note how the two ways of varying the non-additivity affect the depletion potentials differently.

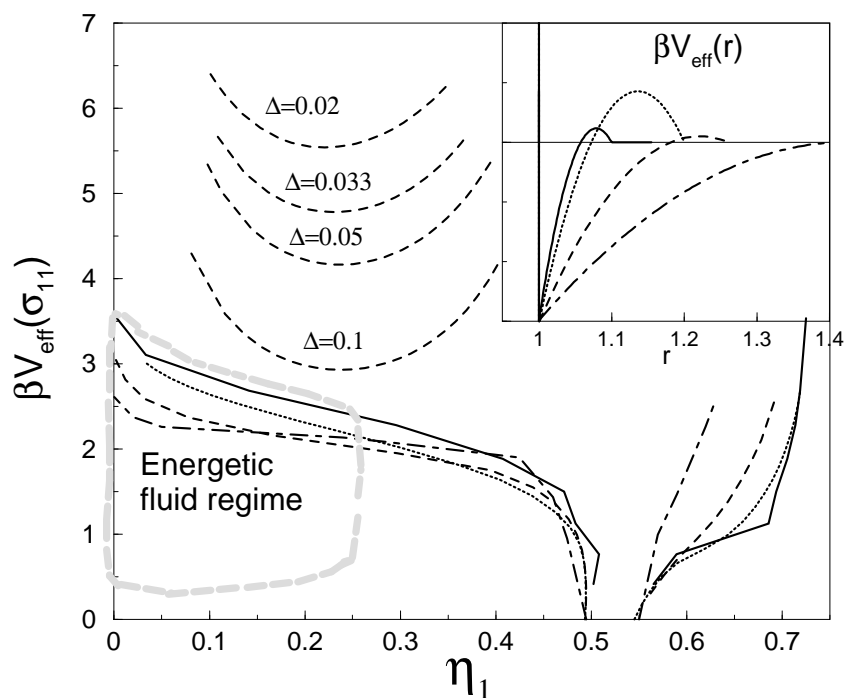


Figure 3. Typical phase-diagram for short-range depletion potential systems. The meta-stable fluid-fluid lines are for depletion potentials with  $y = 0.2$  and different  $\Delta$  (Louis *et al.* 2000a). The fluid-solid lines come from the potentials in the inset (each with corresponding line styles), here normalized to the same minimum at contact. Note the differences in range and shape of the potentials. The area inside the broad dashed lines roughly denotes the stable energetic fluid regime; above the fluid-solid curves would be the metastable energetic fluid regime. The fluid-solid lines for the 3 shorter range potential systems was generated with first order perturbation theory, while the  $y = 0.4$  AO potential fluid-solid line comes from the simulations of Dijkstra *et al.* (1999b) because 1st order perturbation theory incorrectly exhibits a stable fluid-fluid phase-transition.

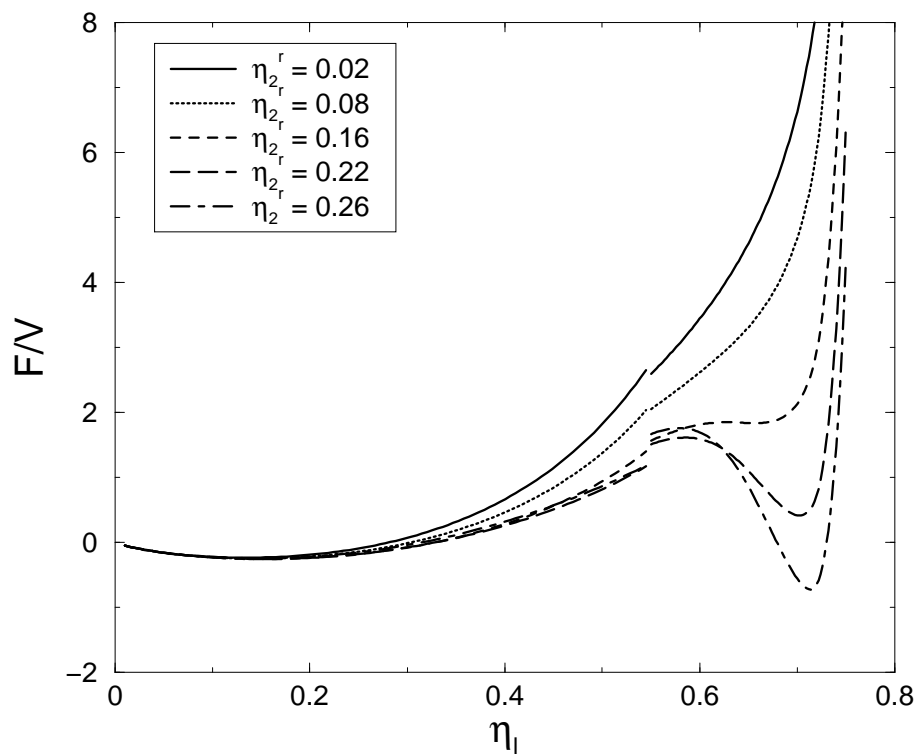


Figure 4. Normalized free energies per unit volume for the additive HS potential used in (Dijkstra *et al.* 1998), at a size-ratio  $y = 0.2$ . The packings of the small-spheres are  $\eta_2^r = 0.02, 0.08, 0.16, 0.22$  and  $0.26$ , which correspond to well-depths of  $\beta V(r = \sigma_1) = 0.183, 0.768, 1.597, 2.224, 2.632$ , respectively. Both branches of the free energy curve decrease with increasing potential well-depth, but the effect is much more pronounced for the crystal branch.

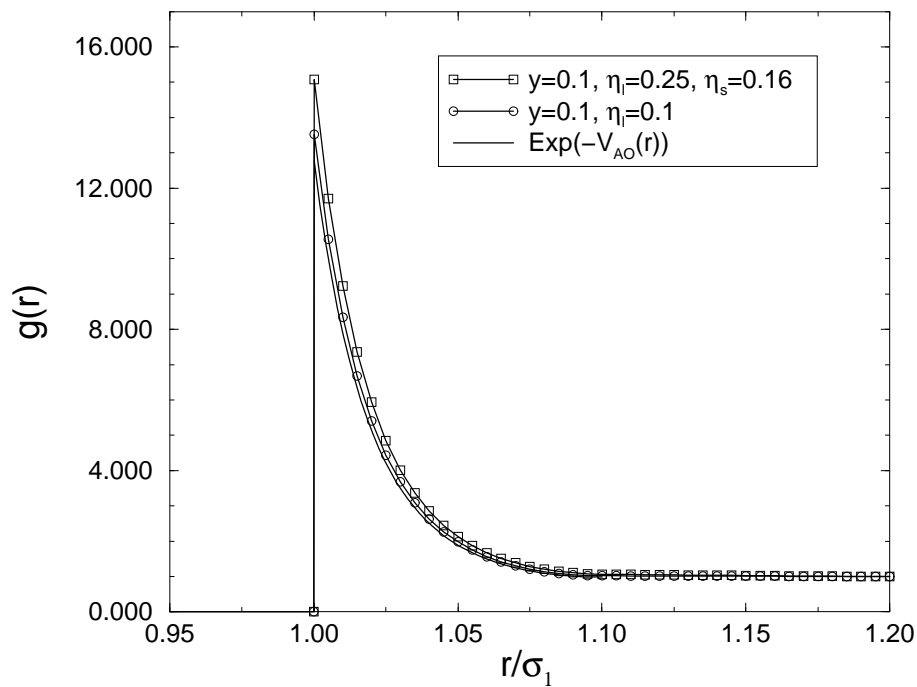


Figure 5. The exponential form  $g(r) = \exp(-\beta V_{AO}(r))$  is a semi-quantitative approximation for these two state-points in the energetic fluid regime. When  $\eta_l = 0.25$ , the system is near the fluid-solid line. The  $g(r)$  were generated with the Percus Yevick (PY) approximation, which is quantitatively accurate in this regime (see e.g. Dijkstra *et al.* 1999b)).

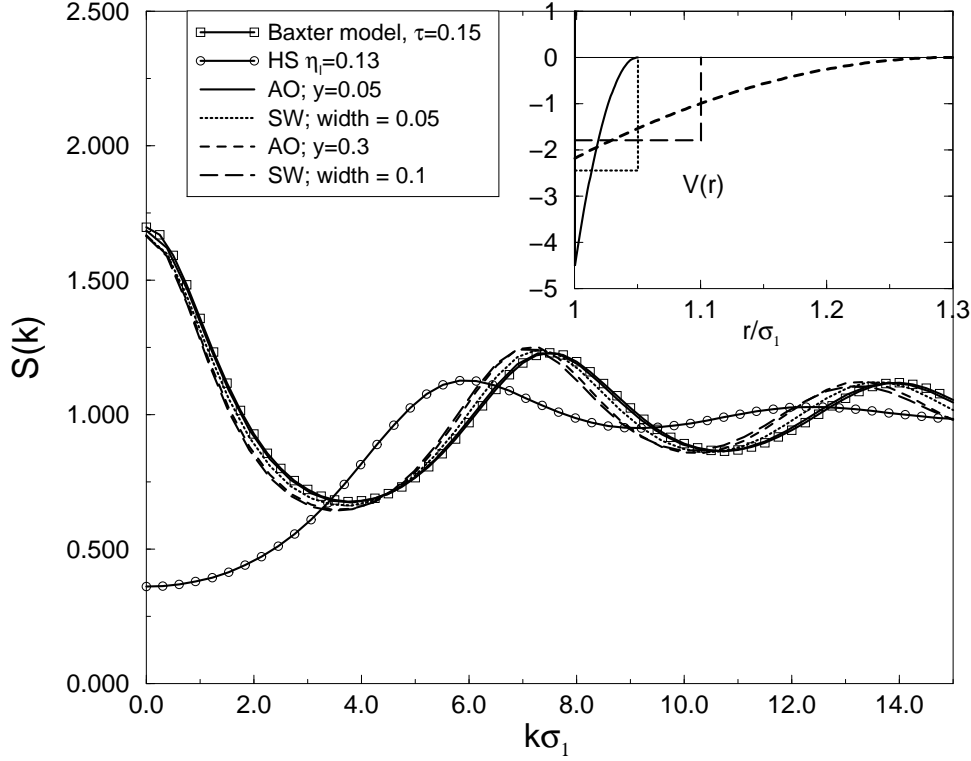


Figure 6. The structure-factors  $S(k)$  at  $\eta_l = 0.13$  for the potentials in the inset. Note that the shape of  $S(k)$  is poorly approximated by the pure hard-sphere form, but well represented by the Baxter model  $S(k)$ . The two shorter range potentials have the same  $B_2$  as the Baxter model, while the two longer range potentials have a  $B_2$  about 7% more negative, which fits to almost the same  $S(0)$ . The differences in the  $S(k)$  due to the shape and range of the potentials are not much larger than the resolution of the best experiments on colloids in solution. As in the previous figure, the  $S(k)$  were determined by the accurate PY approximation.

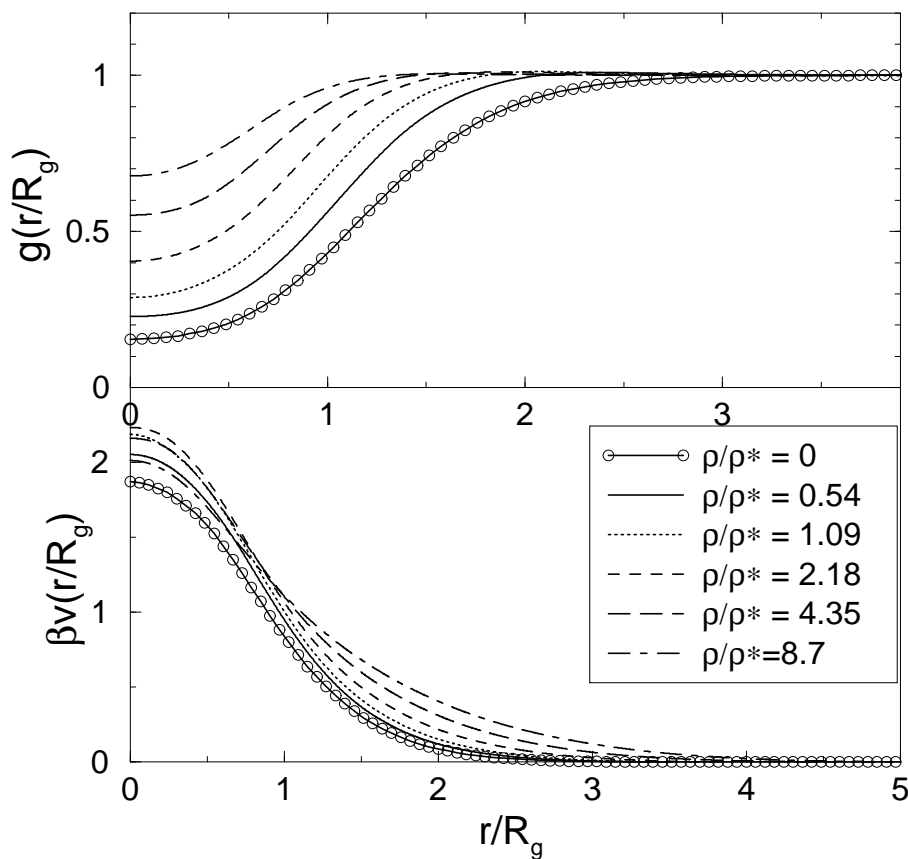


Figure 7. MC simulations are used to generate the  $g(r)$  for  $L = 500$  SAW polymer chains on a cubic ( $240^3$ ) lattice for densities from  $\rho \approx 0$  ( $N = 2$  polymers) to  $\rho/\rho^* = 8.7$ , ( $N = 6400$ ) Here  $\rho^* = 4/3\pi R_g^3$ , and  $\rho/\rho^* < 1$  denotes the dilute and  $\rho/\rho^* > 1$  the semi-dilute regimes for polymers in a good solvent. These radial distribution functions are inverted using an Ornstein-Zernike procedure to obtain the effective potentials between the polymer CM.

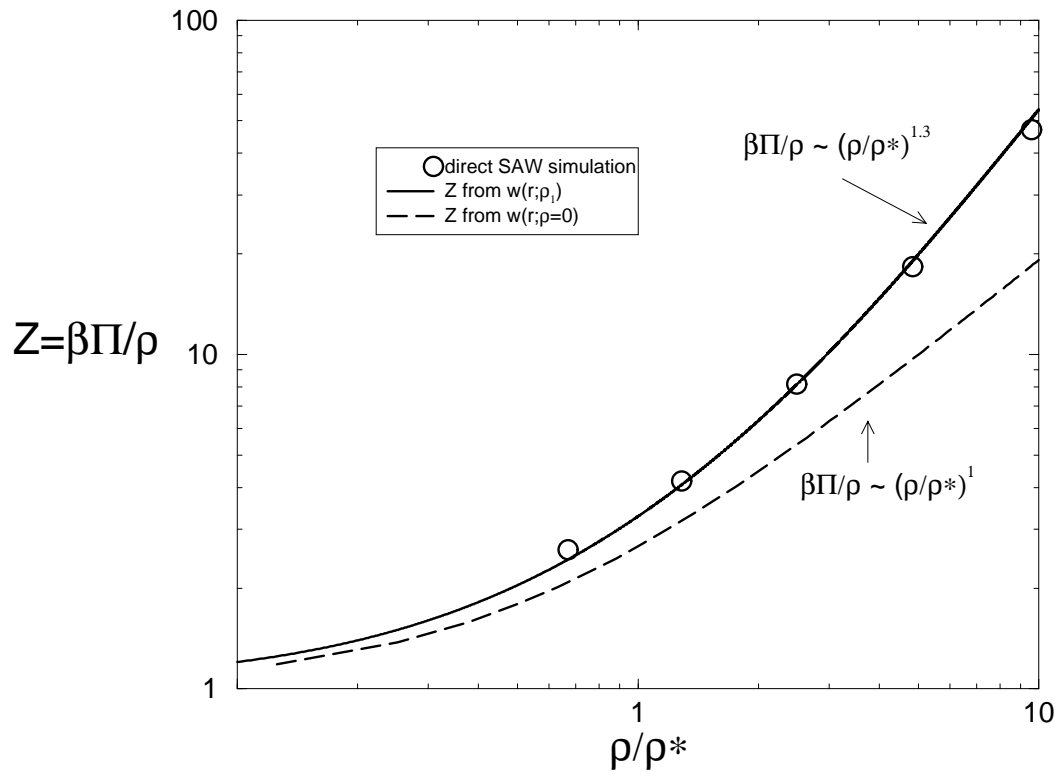


Figure 8. The equation of state derived from the compressibility relation (A 9) accurately approximates the true EOS measured by direct simulations of the polymers. This implies that the volume terms are small. Ignoring the density dependence of the potentials by using only the low density form of the pair potential,  $w(r; \rho = 0)$ , equivalent to the pair-contribution to the EEP, leads to an underestimate of the pressure

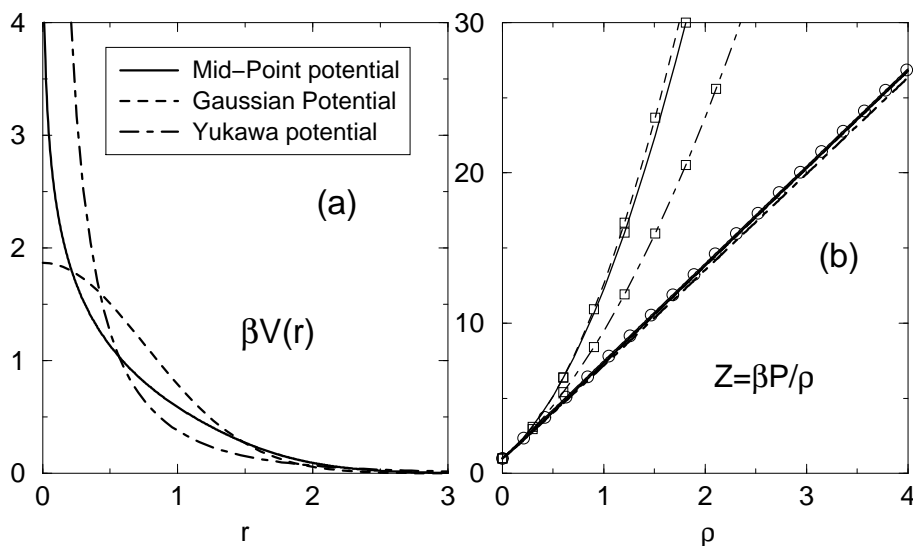


Figure 9. (a): Three potentials  $\beta V(r)$  which all result in a mean field fluid. (b): The EOS  $Z = \beta P/\rho$ , here generated by the quantitatively accurate HNC approximation, are all very close to the  $Z_{MF}$  (equation (4.2)) form (circles). However they are badly approximated by a third order virial series  $Z = 1 + B_2\rho + B_3\rho^2$ , here represented by squares along each line. In this and the next two plots, line styles in (a) and (b) denote corresponding systems.

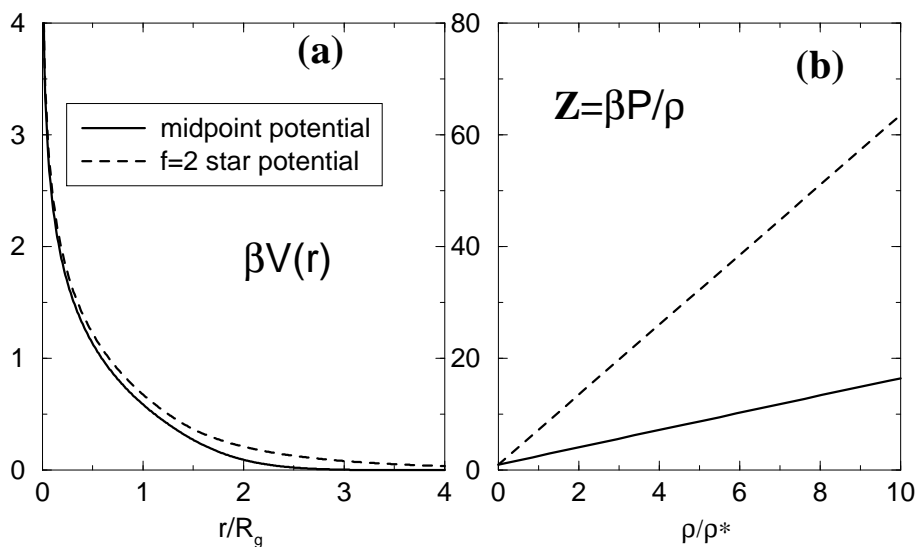


Figure 10. (a) Comparison of two very similar looking potentials that describe the midpoint–midpoint interaction. (b) Note how different their EOS are!

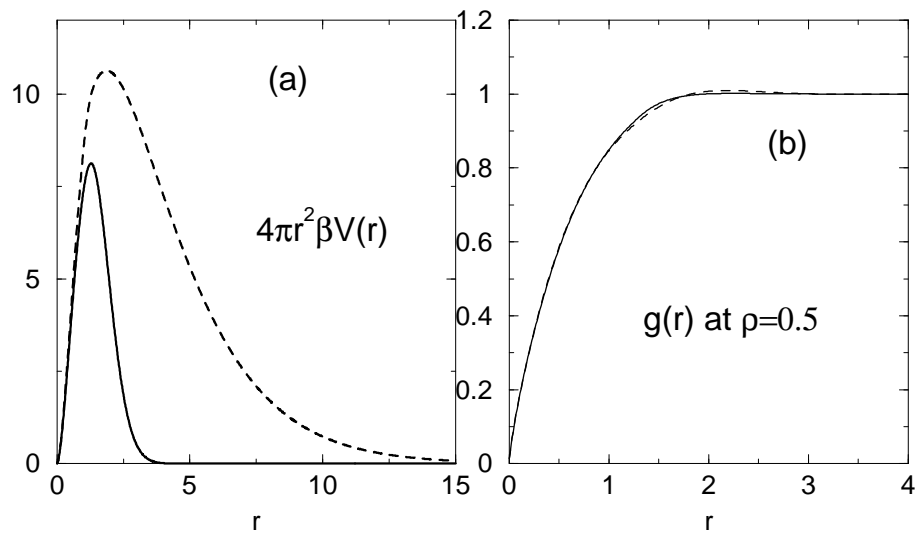


Figure 11. (a) The differences between the two mid-point potentials in the previous figure become much more apparent when they are multiplied by  $r^2$ . (b) This does not translate into much difference in the  $g(r)$  shown here for  $\rho = 0.5$ , but  $S(k)$  (not depicted here) does change.

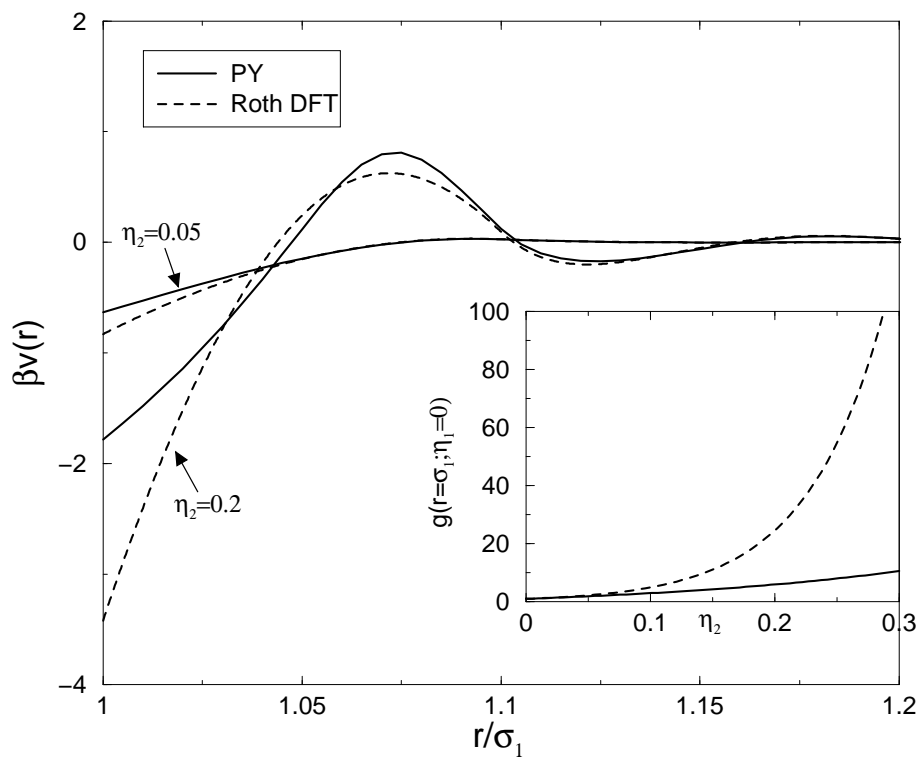


Figure 12. Comparison of the depletion potential  $w^{(2)}(r; \rho_2)$  derived from the PY approximation and from the quantitatively accurate Roth DFT method discussed in the text. PY tends to underestimate the potential strength, leading to a much reduced contact value of  $g_{11}(r)$  in the  $\rho_1 \rightarrow 0$  limit, as shown in the inset.